remote sensing

MDPI

Article

Multi-Scale Assessment and Prediction of Drought: A Case Study in the Arid Area of Northwest China

Tingting Pan [1,2], Yang Wang [1,*], Yaning Chen [2], Jiayou Wang [2,3] and Meiqing Feng [2,3,4]

[1] Ministry of Education Key Laboratory for Western Arid Region Grassland Resources and Ecology, Xinjiang Agricultural University, Urumqi 830052, China
[2] Key Laboratory of Ecological Safety and Sustainable Development in Arid Lands, Xinjiang Institute of Ecology and Geography, Chinese Academy of Sciences, Urumqi 830011, China; chenyn@ms.xjb.ac.cn (Y.C.)
[3] University of Chinese Academy of Sciences, Beijing 100049, China
[4] Graduate School of Environmental Studies, Tohoku University, Sendai 980-8572, Japan
* Correspondence: wangyang@xjau.edu.cn

Highlights

What are the main findings?

- Warming in the Arid Area of Northwest China offsets the humidification effect caused by increased precipitation.
- Multi-model integration significantly reduces prediction variance and bias, substantially improving simulation accuracy. Multi-scale SPEI-based projections indicate a continued intensification of meteorological drought in the region.

What is the implication of the main finding?

- The counteracting effect of warming against precipitation-induced humidification reveals an increasingly warm-dry climate trend in arid Northwest China.
- The integration of multiple models provides a more robust and reliable approach for drought prediction, reveals the trend of persistent drought intensification, and offers scientific justification and urgency for formulating adaptive water allocation and drought mitigation strategies.

Abstract

Accurate prediction of meteorological drought is essential for climate adaptation and sustainable water management in arid regions. Using the Standardized Precipitation Evapotranspiration Index (SPEI) derived from 1962–2021 meteorological observations, this study analyzed multi-scale drought evolution in the Arid Area of Northwest China (AANC) and revealed a distinct shift from wetting to drying after the 1997 abrupt warming. Correlation analysis indicated that the rapid temperature rise significantly enhanced evapotranspiration, offsetting the humidification effect of precipitation. To improve predictive performance, a Stacking ensemble framework was developed by integrating Elastic Network, Random Forest, and Prophet + XGBoost models, with the outputs of the base learners serving as inputs to a meta-regression layer. Compared with single models (NSE $\leq$ 0.742), the integrated model achieved superior accuracy (NSE = 0.886, MAE = 0.236, RMSE = 0.214), and its residuals followed a near-normal distribution, indicating high robustness. Future projections for 2022–2035 show consistent declines in $SPEI_1$, $SPEI_3$, $SPEI_6$, $SPEI_{12}$, and $SPEI_{24}$, suggesting that the AANC will experience increasingly frequent and severe droughts as warming-induced evaporation continues to outweigh the humidification effect of precipitation. This integrated framework enhances drought predictability and provides theoretical support for climate risk assessment and adaptive water management in arid environments.

check for updates

Academic Editor: Liang Sun

Received: 3 November 2025
Revised: 30 November 2025
Accepted: 9 December 2025
Published: 10 December 2025

Citation: Pan, T.; Wang, Y.; Chen, Y.; Wang, J.; Feng, M. Multi-Scale Assessment and Prediction of Drought: A Case Study in the Arid Area of Northwest China. *Remote Sens.* **2025**, *17*, 3985. https://doi.org/10.3390/rs17243985

Copyright: © 2025 by the authors. Licensee MDPI, Basel, Switzerland. This article is an open access article distributed under the terms and conditions of the Creative Commons Attribution (CC BY) license (https://creativecommons.org/licenses/by/4.0/).

Keywords: standardized precipitation evapotranspiration index; drought prediction; model integration; Arid Area of Northwest China

1. Introduction

Drought is one of the most complex and devastating natural hazards, tightly linked to key components of the terrestrial water cycle such as precipitation, evapotranspiration, infiltration, and runoff [1,2]. Due to its far-reaching ecological and socioeconomic impacts, drought has been recognized as a central research theme in several international programs, including the Global Land Project (GLP), the Global Water System Project (GWSP), and the Integrated Land Ecosystem–Atmosphere Processes Study (iLEAPS). The United Nations Environment Programme (UNEP) has also identified drought as one of the most critical environmental challenges of the twenty-first century [3,4]. According to the Global Drought Number Report 2024, the frequency and duration of global droughts have increased by 29% and 31%, respectively, since 2000, with more than 2.3 billion people worldwide now facing drought-induced water scarcity [5,6]. These prolonged events exert severe impacts on ecosystems, food security, and livelihoods, resulting in annual global economic losses exceeding 7 billion USD [7,8].

Under the combined influence of climate change and intensified human activities, global arid and semi-arid regions are continuously expanding, particularly in developing countries with fragile socioeconomic systems [9,10]. The IPCC Sixth Assessment Report confirms a general upward trend in drought frequency and severity, driven by rising temperatures and altered precipitation regimes [11]. This warming-induced increase in evaporative demand has led to a global "dry-getting-drier, wet-getting-wetter" pattern, further amplifying hydrological imbalances [12,13]. It is projected that, by the mid-21st century, drought-related water scarcity and reduced crop productivity may force up to 216 million people to migrate [14,15]. Consequently, understanding the mechanisms of drought evolution and developing reliable prediction systems have become urgent global priorities—especially in inland arid regions where water resources are extremely limited.

Accurate drought prediction is fundamental for adaptive water resource management and agricultural planning in water-scarce regions [16–18]. Traditionally, statistical approaches such as regression analysis, autoregressive time series models, Markov chains, and conditional probability models have been applied to forecast droughts based on historical hydroclimatic records [19–23]. In recent years, artificial intelligence (AI) and machine learning (ML) techniques have been increasingly used to enhance prediction performance [24–26]. However, single-model approaches often struggle to extract complex nonlinear relationships or to adapt to non-stationary time series, resulting in underfitting and limited generalization in changing climatic conditions [27–29].

Model integration provides a promising solution by combining the complementary strengths of different algorithms [30]. Ensemble learning frameworks—typically represented by Bagging and Boosting—have been widely adopted to improve model robustness and reduce bias [31]. Among these, Random Forest (RF) effectively captures nonlinear dependencies through multiple decision trees, while Gradient Boosting Decision Tree (GBDT) and its optimized version, Extreme Gradient Boosting (XGBoost), achieve high computational efficiency and strong generalization through iterative residual learning and regularization [32–34]. Despite these advantages, conventional ensemble methods still face challenges in representing the chaotic behavior of atmospheric processes and the large variability of short-term drought indices [35]. Ensemble and stacking strategies

that combine complementary algorithms have therefore emerged as a promising route to improve robustness and predictive skill.

To address the above limitations, in this study, we develop and evaluate a Stacking ensemble framework for multi-scale meteorological drought assessment and prediction in the Arid Area of Northwest China (AANC). We use long-term ground observations (1962–2021) to compute multi-scale SPEI (1–24 months), and complement station data with reanalysis and climate model datasets for independent verification. Three base learners—Elastic Net, Random Forest, and Prophet combined with XGBoost—are trained to simulate SPEI, and their outputs are fused by a regression meta-learner to produce ensemble forecasts. Our objectives are to: (1) diagnose historical changes and abrupt transitions in AANC drought regimes across multiple time scales; (2) quantify how integrating multiple learners affects predictive accuracy compared with single models; and (3) project SPEI trajectories through 2035 to assess near-term drought risk under continued warming.

2. Materials and Methods

2.1. Study Area

The Arid Area of Northwest China (AANC) is one of the most representative inland arid regions in the world, covering approximately 2.5 × 10^6 km^2 between 73–107°E and 34–50°N. It spans Xinjiang, the Hexi Corridor of Gansu, Ningxia, the northern Qilian Mountains in Qinghai, and western Inner Mongolia (Figure 1). The terrain ranges from −154 m in the Turpan Depression to over 5500 m in the Kunlun–Tianshan–Qilian mountain systems, forming sharp climatic and hydrological gradients.

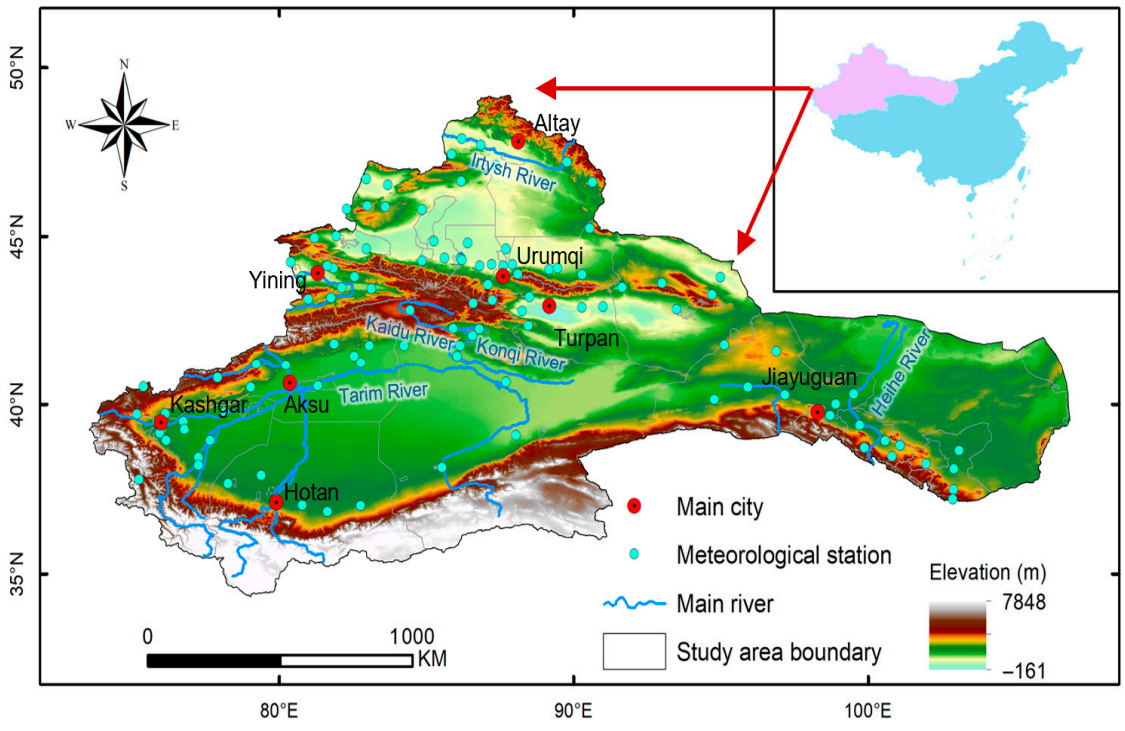


Figure 1. Map of study area.

The region contains several major inland river basins—such as the Tarim River, Heihe River, Shiyang River, and Ili River—which are primarily sustained by mountain precipitation, glacier meltwater, and seasonal snowmelt. Key oasis cities, including Urumqi, Kashgar, Korla, Yinchuan, Zhangye, and Dunhuang, are concentrated along these river corridors, where limited but stable water supplies enable agriculture and settlement. Al-

though oases account for barely 10% of the total land area, they support the majority of socioeconomic activities in the AANC [36].

Climatically, the AANC sits at the interface of the mid-latitude westerlies and the Asian summer monsoon, resulting in strong spatial contrasts in precipitation and temperature. Mean annual temperature ranges from 5 to 14 °C, while precipitation decreases drastically from approximately 500 mm in the surrounding mountains to less than 20 mm in the central basins. More than 80% of the region is hyper-arid to semi-arid, with extremely high potential evapotranspiration (1500–2800 mm yr^{-1}) and low aridity indices (AI = 0.03–0.20). These conditions create a fragile eco-hydrological system highly sensitive to climatic perturbations [37].

Historically, the AANC has experienced multiple severe droughts. Notable events occurred in 1979–1982, 1985–1987, 1999–2002, and 2006–2008, each leading to sharp declines in river runoff, widespread agricultural losses, and regional ecological degradation. Long-term observations show rapid warming since the late 1950s (0.4–0.6 °C $decade^{-1}$) accompanied by modest increases in precipitation (1–3 mm $decade^{-1}$), producing a heterogeneous but notable warming–wetting trend [38]. The region's complex terrain, scarce water resources, and high climate sensitivity make it a key natural laboratory for understanding drought evolution and developing adaptive water management strategies under ongoing climate change.

2.2. Datasets

Topographic, meteorological, and drought-related datasets were used to support the multi-scale analysis. The 90 m-resolution Digital Elevation Model (DEM) of the Arid Area of Northwest China (AANC) was acquired from the International Scientific Data Service Platform (http://srtm.csi.cgiar.org/, accessed on 1 June 2025) and processed using ArcGIS 10.8 for mosaicking, clipping, and spatial visualization.

Meteorological observations were obtained from 114 national stations across the AANC. Daily temperature and precipitation (1962–2021) were sourced from the China Surface Climatological Data Daily Values (V3.0), released by the National Meteorological Information Center (http://data.cma.cn/, accessed on 15 June 2025). To ensure reliability for drought assessment, a comprehensive quality-control framework was applied prior to analysis:

Outlier detection: A combination of percentile-based range checks and the penalized maximal F-test was used to identify anomalous temperature and precipitation values. Outliers inconsistent with physical or temporal patterns were corrected using neighboring-station analogs.

Homogeneity testing: Statistical tests including Pettitt, SNHT (Standard Normal Homogeneity Test), and Buishand range test were performed to detect breakpoints caused by station relocation, instrument replacement, or observational inconsistencies. Detected inhomogeneities were adjusted based on reference-station series.

Missing-value interpolation: Less than 0.8% of daily records were missing. These were reconstructed using spatiotemporal kriging combined with correlation-weighted interpolation from nearby stations to maintain temporal continuity and spatial consistency.

Based on the processed temperature, precipitation, and PET datasets, the Standardized Precipitation Evapotranspiration Index (SPEI) was computed at 1-, 3-, 6-, 12-, and 24-month scales to characterize drought intensity and temporal evolution.

To enhance robustness, the spatial–temporal patterns of calculated SPEI were cross-checked with ERA5 (https://cds.climate.copernicus.eu/, accessed on 18 June 2025) and CMIP6 (https://pcmdi.llnl.gov/CMIP6/, accessed on 21 June 2025) multi-model ensemble climatology. Their comparable variability and long-term trends provide independent validation supporting the reliability of the station-derived SPEI used in this study (Figure 2).

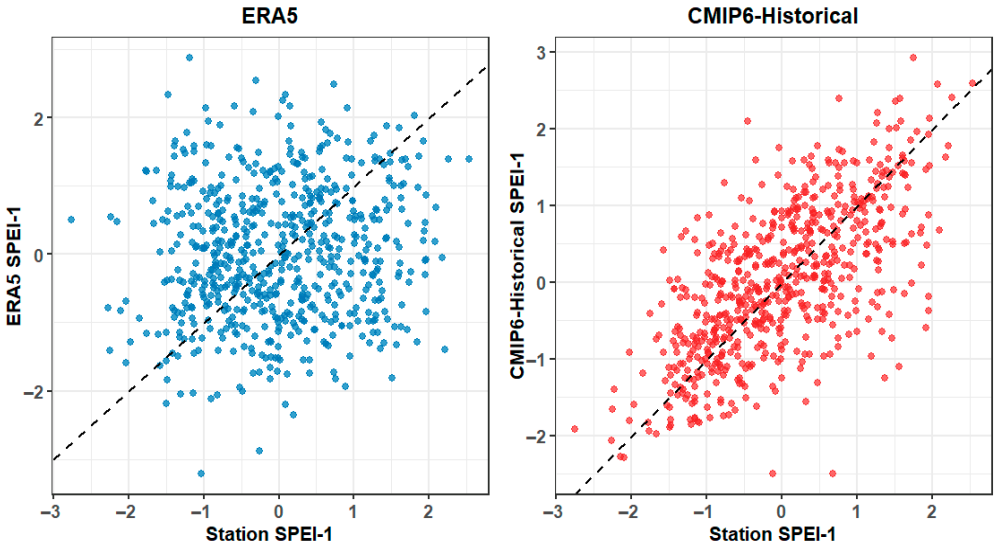


Figure 2. Scatter plot for SPEI data validation.

2.3. Methods

This study establishes an integrated framework combining statistical decomposition, drought index calculation, and machine learning to assess and predict multi-scale meteorological drought in the Arid Area of Northwest China (AANC). First, long-term temperature and precipitation series are decomposed using the BEAST algorithm to identify abrupt changes, seasonal variations, and long-term trends in key climatic variables. Second, the Standardized Precipitation Evapotranspiration Index (SPEI) is calculated at multiple time scales based on precipitation and potential evapotranspiration derived from the Penman–Monteith equation, capturing the characteristics of drought evolution. Third, three base models—Elastic Net (EN), Random Forest (RF), and Prophet combined with XGBoost—are employed to simulate the linear trends, nonlinear patterns, and seasonal variations of the SPEI series. Finally, a stacked ensemble regression integrates the outputs of these models to improve prediction accuracy and robustness. This framework enables simultaneous detection of nonlinear climatic variations, characterization of multi-scale drought dynamics, and reliable forecasting of future drought conditions (Figure 3).

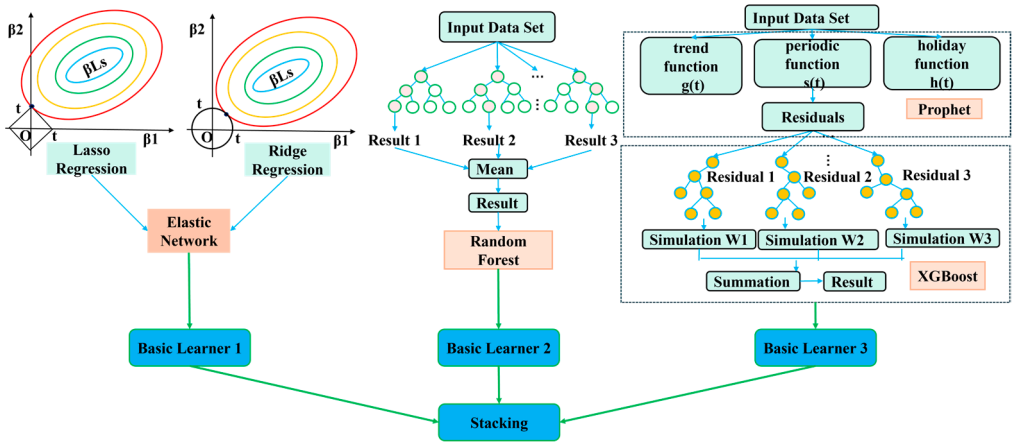


Figure 3. Framework for drought prediction based on model integration.

2.3.1. BEAST

The BEAST (Bayesian Estimator of Abrupt change, Seasonal change, and Trend) algorithm is a robust time series decomposition method that integrates multiple competing models using a Bayesian model averaging framework. By combining the strengths of

individual decomposition models, BEAST can detect abrupt changes (change points), periodic patterns (e.g., seasonality), and arbitrary nonlinear trends in time series data [39,40]. The algorithm not only identifies the timing of changes but also quantifies the statistical confidence that these changes are significant. Unlike conventional piecewise linear approaches, BEAST can capture complex nonlinear trends, making it highly suitable for climate, hydrology, ecology, remote sensing, and economic time series. Detailed calculation formulas and implementation code are available at https://github.com/zhaokg/Rbeast (accessed on 1 June 2025).

2.3.2. SPEI

The Standardized Precipitation Evapotranspiration Index (SPEI) is an extension of traditional univariate drought indices, such as the Standardized Precipitation Index (SPI), with the added advantage of explicitly accounting for temperature-driven changes in atmospheric evaporative demand [41]. By incorporating potential evapotranspiration (PET), SPEI provides a more physically meaningful measure of meteorological drought, particularly under warming climates. Moreover, SPEI can be computed at multiple time scales, enabling the characterization of short-term to long-term drought conditions. The SPEI is calculated by replacing precipitation in the SPI framework with the climatic water balance, defined as the difference between precipitation (P) and PET. This difference is then fitted to a log-logistic probability distribution and standardized to yield the SPEI value. This approach allows both positive (wet) and negative (dry) anomalies to be consistently quantified across scales. In this study, SPEI was computed at 1-, 3-, 6-,12-, and 24-month time scales to capture the multi-scale dynamics of drought in the Arid Area of Northwest China (AANC). The calculation procedure consists of four main steps, as detailed below:

(1) Calculate the climatic water balance, with the climatic water balance (D_i) being the difference between precipitation (P_i) and potential evapotranspiration (PET_i):

$$D_i = P_i - PET_i \tag{1}$$

(2) Establish the cumulative series of climatic water balance at different time scales:

$$D_n^k = \sum_{i=0}^{k-i} (P_{n-i} - PET_{n-i}), n \geq k \tag{2}$$

where k is the time scale (usually month) and n is the number of calculations.

(3) Build a data series using the log-logistic probability density function fitting:

$$f(x) = \frac{\beta}{\alpha}\left(\frac{x-\gamma}{\alpha}\right)^{\beta-1}\left[1+\left(\frac{x-\gamma}{\alpha}\right)^{\beta}\right]^{-2} \tag{3}$$

where α is the scale coefficient, β is the shape coefficient, and γ is the origin parameter, which can be obtained by the L-moment parameter estimation method.

(4) Transform the cumulative probability density into a standard normal distribution to obtain the corresponding SPEI time change sequence:

$$SPEI = w - \frac{c_0 + c_1 w + c_2 w^2}{1 + d_1 w + d_2 w^2 + d_3 w^3} \tag{4}$$

where $w = [-2\ln(P)]^{1/2}$, when $P \leq 0.5$, $P = 1 - F(x)$; when $P > 0.5$, $P = 1 - P_i$, $c_0 = 2.515517$; $c_1 = 0.802853$; $c_2 = 0.010380$; $d_1 = 1.432788$; $d_2 = 0.189\,269$; $d_3 = 0.001308$.

2.3.3. Elastic Network

The Elastic Network (EN) is a regularized regression technique that combines the strengths of ridge regression and the least absolute shrinkage and selection operator (LASSO). It introduces a penalty term that is a convex combination of the L1 and L2 norms, effectively balancing variable selection and coefficient shrinkage. The penalty is controlled by two parameters: λ, which determines the overall strength of regularization, and ρ, which defines the relative contribution of the L1 and L2 penalties [42]. When ρ = 0, the EN reduces to ridge regression, while ρ = 1, it becomes equivalent to LASSO.

Due to the non-differentiability introduced by the L1 term, model coefficients are estimated iteratively using the coordinate descent algorithm. EN is particularly suitable for datasets with highly correlated predictors or when the number of predictors exceeds the number of observations, which is common in climate and hydrological studies where multicollinearity among meteorological variables exists [43].

In this study, the EN model was implemented in R using the "glmnet" package. Hyperparameters were set as λ = 0.01 (regularization strength) and ρ = 0.5 (mixing parameter between L1 and L2), which were selected based on preliminary testing and literature-informed defaults to balance model complexity and predictive performance. The model was trained on preprocessed SPEI time series features extracted from meteorological observations, capturing long-term trends and short-term variability.

The objective function of EN is expressed as:

$$\min_{w} \frac{1}{2n} \sum_{i=1}^{n} \left(y_i - \mathrm{x}_i^{\top} w\right)^2 + \lambda \left(\rho \| w \|_1 + \frac{1-\rho}{2} \| w \|_2^2 \right) \quad (5)$$

where y_i is the response variable, x_i is the predictor vector, w is the coefficient vector, n is the number of observations, and $\| w \|_1$ and $\| w \|_2$ denote the L1 and L2 norms, respectively.

This implementation ensures robust prediction of multi-scale SPEI, taking advantage of EN's ability to handle multicollinearity and reduce overfitting in climate time series forecasting.

2.3.4. Random Forest

The Random Forest (RF) algorithm is an ensemble learning method that constructs a large number of decision trees based on bootstrap aggregation (Bagging) [44]. Each tree is trained on a bootstrap sample of the dataset, and the ensemble prediction is obtained by averaging the outputs of all trees, thereby reducing variance and improving model stability. RF is a non-parametric method capable of capturing complex nonlinear relationships and high-order interactions among predictors, making it particularly suitable for hydro-climatic applications that involve heterogeneous and multi-scale environmental variables.

An important feature of RF is the use of out-of-bag (OOB) samples, which serve as an internal cross-validation mechanism to provide an unbiased estimate of prediction error and model generalization ability. Furthermore, RF naturally handles high-dimensional feature sets without requiring dimensionality reduction and provides measures of variable importance, which is useful for interpreting the dominant drivers of SPEI variability.

In this study, the RF model was implemented in R using the "randomForest" engine within the tidymodels/modeltime framework. We explicitly configured two key hyperparameters based on sensitivity testing and widely adopted defaults for time-series regression: Number of trees (trees) = 500, which ensures stable ensemble performance while avoiding overfitting. Minimum node size (min_n) = 50: controls tree depth to prevent overly complex trees and improves generalization for climate time-series data. These tuning choices balance model flexibility and computational efficiency, and they align with best practices for long-term drought index prediction. The model was trained using engineered time-

series features (e.g., seasonal signatures, Fourier terms) extracted from the meteorological dataset, allowing RF to learn nonlinear patterns and multi-scale dependencies embedded in SPEI sequences.

Overall, the RF implementation provides a strong nonlinear benchmark model and serves as one of the three base learners in the stacking ensemble framework used later in this study.

2.3.5. Prophet with XGBoost

Prophet is an open-source forecasting framework developed by Facebook, implemented in both Python and R (https://facebook.github.io/prophet). It decomposes a time series into interpretable components, modeling the signal $y(t)$ as:

$$y(t) = g(t) + s(t) + h(t) + e_t \quad (6)$$

where $g(t)$ represents long-term trend changes, $s(t)$ denotes seasonal components of different periodicities, and $h(t)$ rcaptures holiday or event-related effects occurring at irregular intervals. The error term e_t accounts for unexplained fluctuations and is assumed to follow a Gaussian distribution. Prophet is particularly suitable for long-term climate and hydrological series because of its ability to accommodate multiple seasonalities and abrupt structural changes.

Extreme Gradient Boosting (XGBoost), on the other hand, is an efficient gradient-boosting algorithm that constructs a sequence of decision trees to iteratively minimize residual errors [45]. Its regularization design and shrinkage strategy significantly reduce overfitting while capturing complex nonlinear relationships—properties that are valuable for modeling residual patterns commonly present in meteorological drought series.

In this study, Prophet was first applied to generate baseline predictions for each SPEI time series. The residuals (i.e., observed minus predicted values) were then extracted and modeled using XGBoost to capture additional nonlinear dynamics and short-term dependencies not accounted for by Prophet. The corrected residual predictions were added back to the original Prophet estimates to produce a hybrid Prophet–XGBoost forecast. This two-stage approach enhances both long-term trend fitting and short-term variability representation.

To ensure optimal model performance, hyperparameters in both Prophet and XGBoost were tuned using a structured grid-search procedure, including: for Prophet: changepoint prior scale, seasonality prior scale, and yearly seasonality mode; for XGBoost: number of trees, learning rate, max depth, subsample rate, and column sampling rate. The parameter combination yielding the lowest validation error in the training–testing split was selected as the final configuration. This hybrid modeling strategy significantly improved predictive accuracy and robustness for multi-scale SPEI simulations.

2.3.6. Stacking Ensemble Model

To further enhance the predictive performance and generalization ability, a stacking ensemble learning framework was employed to integrate the outputs of the base learners. Stacking is a two-level learning architecture in which multiple base models are trained independently at the first level, and their prediction outputs are subsequently used as input features for a meta-learner at the second level [46,47]. This meta-learner, typically a multiple linear regression model in this study, learns how to optimally combine the strengths of individual base models to produce more accurate and stable predictions. Specifically, the results generated by the Elastic Network, Random Forest, and Prophet + XGBoost models were used as input variables for the meta-regression model, which then performed secondary learning to capture the residual information and model complementarities among the base learners. This hierarchical integration framework effectively reduces the

bias of single models and the variance of ensemble predictions, thereby improving the overall simulation and forecasting performance of the SPEI time series.

3. Results

3.1. Warming and Humidification Trend Based on Temperature and Precipitation

Both annual temperature and precipitation in the AANC show a significant upward trend from 1962 to 2021 (Figure 4). Despite the overall increase, the time series exhibit marked interannual and multi-decadal fluctuations. A sharp rise in precipitation is detected around 1987, followed by a pronounced warming shift approximately a decade later in 1997. These change points correspond to distinct climate phases: a cold–dry period during 1962–1987, a short cold–wet interval in 1988–1996, and a warm–wet regime after 1997. The concurrent increases in both temperature and precipitation confirm a persistent warming and humidification trajectory across the AANC over the past six decades.

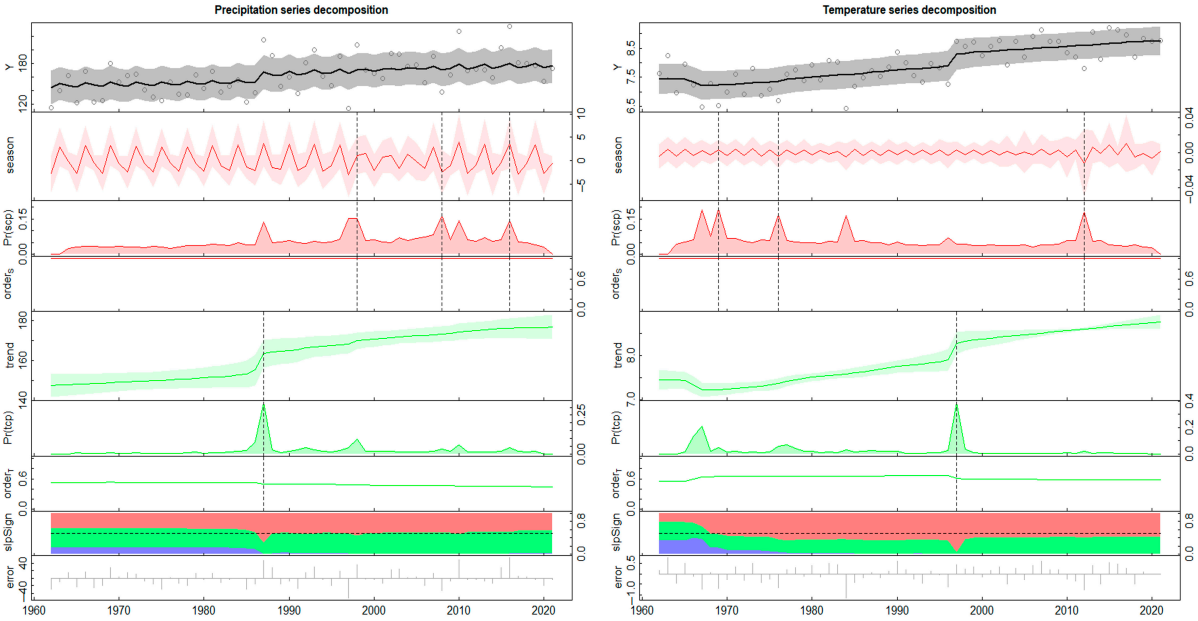


Figure 4. BEAST decomposition of temperature and precipitation series. Y represents the original precipitation or temperature time series. Season denotes the seasonal or periodic component; Pr(scp) indicates the probability of seasonal changepoint occurrence, and orderS refers to the time-varying polynomial order used to fit the seasonal component. Trend represents the long-term trend; Pr(tcp) indicates the probability of trend changepoint occurrence, and orderT refers to the time-varying polynomial order used to fit the trend component. slpSign shows the probabilities of the trend slope being positive (red), zero (green), or negative (blue). Error denotes the residual component after decomposition.

3.2. Meteorological Drought Intensification Based on Multi-Scale SPEI

Meteorological drought arises when atmospheric water demand exceeds water supply due to precipitation–evapotranspiration imbalances. To characterize its variability across the AANC from 1962 to 2021, we employed the multi-scale Standardized Precipitation Evapotranspiration Index (SPEI), which incorporates temperature-driven evapotranspiration effects and captures drought conditions over different accumulation periods. According to the SPEI-based drought classification (Table 1), the temporal evolution of drought shows clear phase transitions that correspond to the identified temperature–precipitation change points, allowing the study period to be divided into three distinct phases.

Table 1. Meteorological Drought Rating.

Rating	Drought Type	SPEI
1	Mild drought	$-1 < \text{SPEI} \leq -0.5$
2	Moderate drought	$-1.5 < \text{SPEI} \leq -1$
3	Severe drought	$-2 < \text{SPEI} \leq -1.5$
4	Extreme drought	$\text{SPEI} \leq -2$

During 1962–1987, short-term ($SPEI_1$, $SPEI_3$, $SPEI_6$) and long-term ($SPEI_{12}$) indices generally fluctuated within the range of −1 to 1, with mean values close to zero, indicating relatively balanced hydroclimatic conditions and rare occurrences of extreme drought or wetness. Between 1988 and 1996, all SPEI indices exhibited a marked positive shift, suggesting a transient humid phase consistent with the regional "cold–wet" stage. After 1997, however, SPEI values across all time scales declined significantly, with their range extending to −2, reflecting an increased frequency and intensity of drought events. From an overall perspective, all time-scale SPEIs display a negative linear trend, with the decline becoming steeper at longer accumulation periods. This indicates that long-term water deficits have intensified more strongly than short-term fluctuations, signifying a persistent and scale-dependent enhancement of meteorological drought across the AANC since the late 1990s (Figure 5).

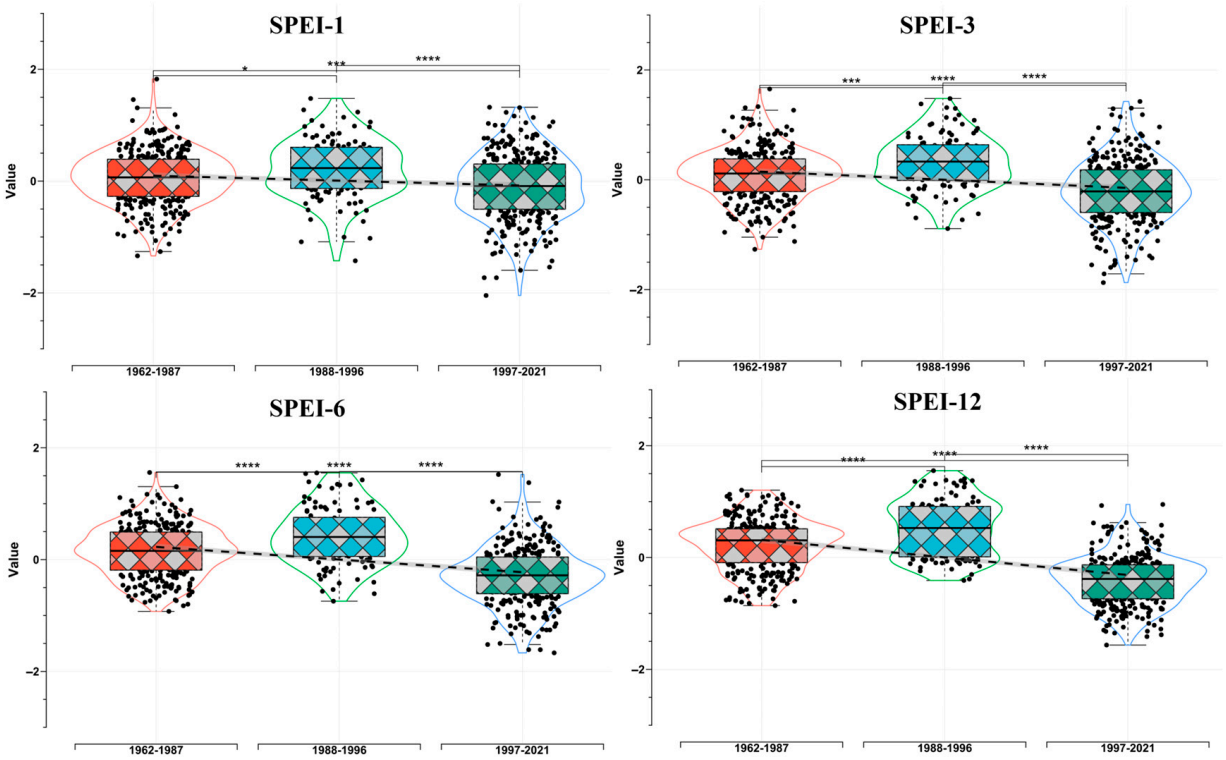


Figure 5. Multi-scale SPEI for different time periods. Note: Asterisks denote statistical significance: * $p < 0.05$; *** $p < 0.01$; **** $p < 0.0001$.

3.3. Warming Offsets the Humidification Effect of Precipitation

To quantify the relative contributions of temperature and precipitation to drought dynamics, we analyzed correlations between these variables and multi-scale SPEI series, using 1997 as the threshold for abrupt warming. Before 1997, precipitation was strongly positively correlated with $SPEI_1$, $SPEI_3$, $SPEI_6$, and $SPEI_{12}$, with correlation coefficients of 0.45, 0.37, 0.29, and 0.13, respectively (Figure 6a), indicating a dominant humidifying effect

of precipitation. Temperature correlations with SPEI were weak and positive, suggesting a minor influence on drought during this period.

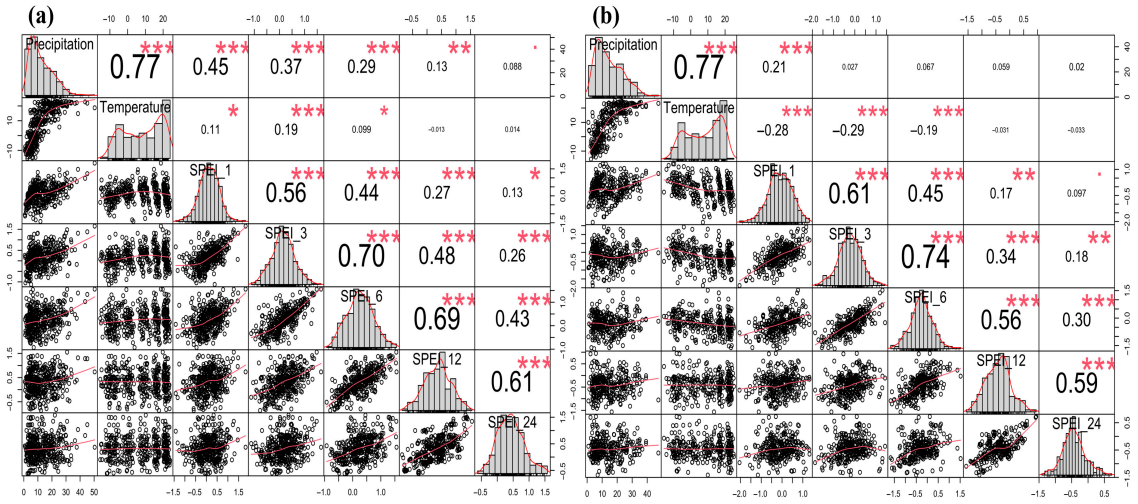


Figure 6. Correlation coefficients between temperature, precipitation, and multi-scale SPEI before and after the 1997 abrupt warming: (**a**) correlations during the pre-warming period (1962–1996); (**b**) correlations during the post-warming period (1997–2021). Note: Asterisks denote statistical significance: * $p < 0.05$; ** $p < 0.01$; *** $p < 0.001$.

After the 1997 warming shift, the correlation pattern changed markedly (Figure 6b). Precipitation remained moderately positively correlated only with short-term $SPEI_1$, while correlations with longer-scale SPEIs became insignificant. In contrast, temperature was negatively correlated with $SPEI_1$, $SPEI_3$, and $SPEI_6$ (-0.28, -0.29, and -0.19), highlighting that increased evaporative demand under warming offset the humidification effect of precipitation. These results indicate a transition toward a "warm–dry" hydroclimatic regime, where the drying effect of increased evaporative demand outweighed precipitation gains. Importantly, this drying reflects the integrated effect of temperature, precipitation, and evapotranspiration, rather than contradicting the warming–humidification trend inferred from temperature and precipitation alone.

3.4. Multi-Model Simulation and Prediction of SPEI

Analysis of historical observations confirms that the Arid Area of Northwest China (AANC) has experienced a continuous warming and humidification trend. Climate model simulations further project that ongoing greenhouse gas and sulfate aerosol emissions will continue to intensify regional warming and increase precipitation. However, higher temperatures drive strong increases in evapotranspiration, resulting in considerable uncertainty regarding future drought conditions as represented by the Standardized Precipitation Evapotranspiration Index (SPEI). Quantitative simulation and prediction of SPEI are therefore essential to assess the balance between warming, humidification, and enhanced drying effects. Three base learners—Elastic Net (EN), Random Forest (RF), and Prophet combined with XGBoost—were first applied to simulate multi-scale SPEI series (Figure 7). Each model exhibits distinct predictive characteristics: EN effectively captures the overall trend but underestimates nonlinear fluctuations; RF identifies partial periodic structures but underestimates long-term variability; and Prophet + XGBoost accurately fits short-term volatility but tends to underestimate extreme drought and wetness events. These complementary behaviors form the basis for ensemble integration to enhance robustness and predictive accuracy.



Figure 7. SPEI basic model simulation results. Note: EN refers to Elastic Network, and RF refers to Random Forest.

The three base learners were then combined using a Stacking ensemble framework, where outputs from the base models serve as input features to a meta-learner implemented as multiple linear regression. This approach leverages the complementary strengths and diversity of the base learners to improve overall prediction performance. Predictive performance was quantitatively evaluated using Mean Absolute Error (MAE), Root Mean Square Error (RMSE), and Nash–Sutcliffe Efficiency (NSE) (Table 2). As shown in Figure 8a, the Stacking ensemble achieved substantial improvements over individual models, effectively reducing bias and variance. Residual analysis (Figure 8b) demonstrates that errors are approximately normally distributed with a mean near zero, indicating good calibration and unbiased predictions.

Application of the ensemble model to forecast SPEI for 2022–2035 shows a consistent declining trend across all time scales ($SPEI_1$, $SPEI_3$, $SPEI_6$, $SPEI_{12}$, and $SPEI_{24}$), suggesting a progressive intensification of meteorological drought in the AANC (Figure 9). Longer accumulation periods exhibit wider confidence intervals, reflecting increased uncertainty and a higher likelihood of extreme drought events in the long term. These results highlight the complex interplay between warming, precipitation, and evapotranspiration in shaping future drought risks.

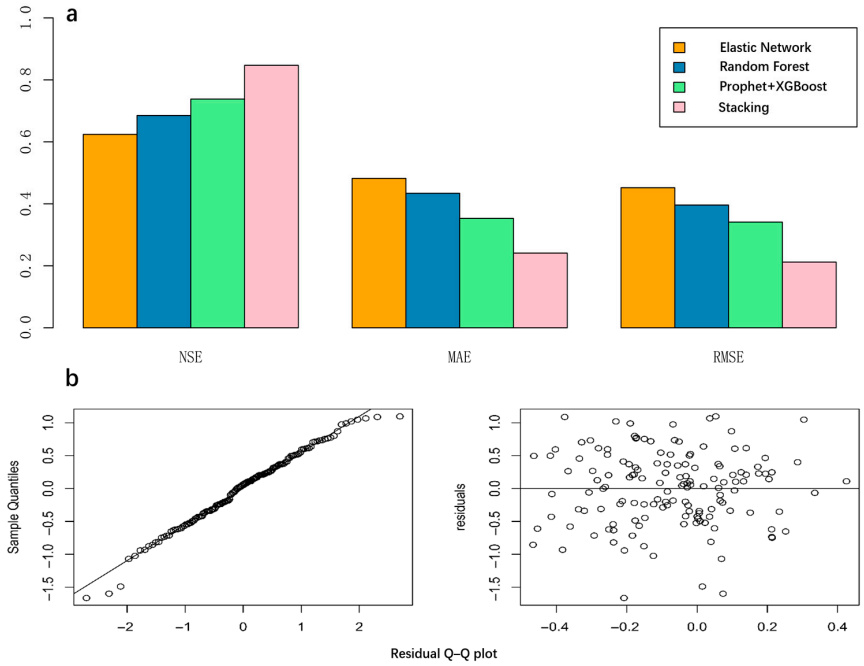


Figure 8. Comparison of model performance and residual analysis: (**a**) Predictive accuracy of different models, quantified by Nash–Sutcliffe Efficiency (NSE), Mean Absolute Error (MAE), and Root Mean Square Error (RMSE); (**b**) Q–Q plot of residuals after Stacking ensemble integration, showing approximate normality with a mean near zero.

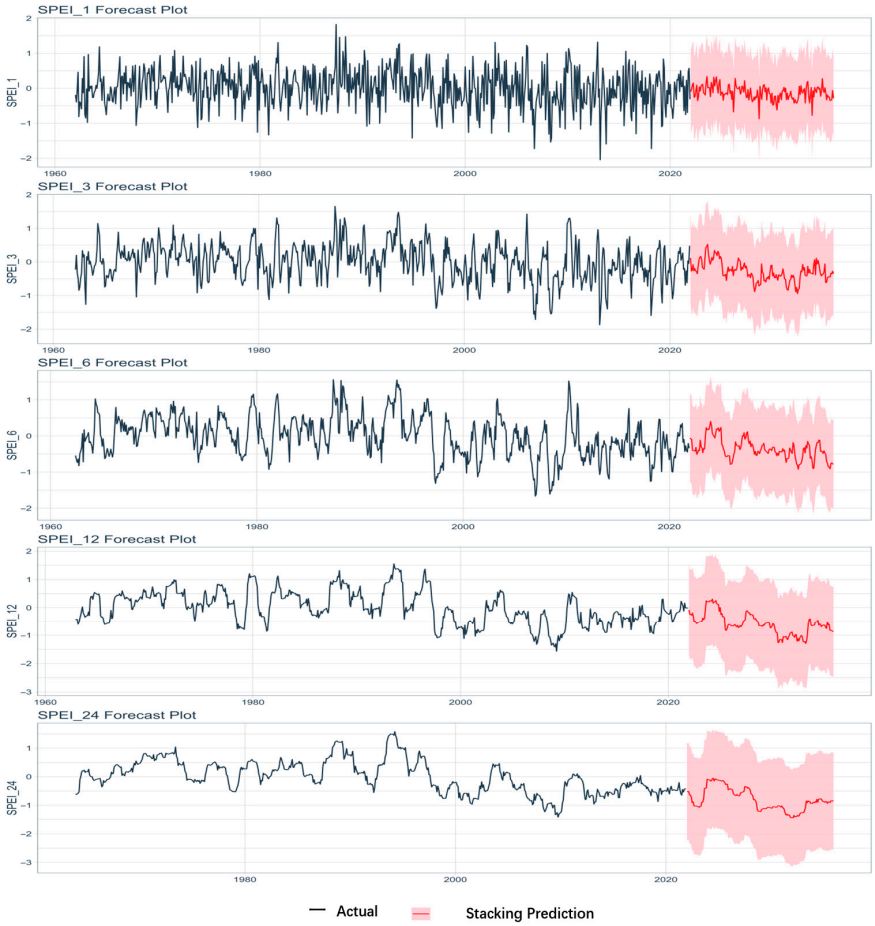


Figure 9. Multi-scale SPEI ensemble prediction in the Arid Area of Northwest China during the historical period (1962–2021) and the projected period (2022–2035).

Table 2. Model Evaluation Index.

Index	Equation	Range of Index	Optimum Value
NSE	$NSE = 1 - \frac{\sum_{i=1}^{n}\left(X_{obs}^{i} - X_{sim}^{i}\right)^2}{\sum_{i=1}^{n}\left(X_{obs}^{i} - \overline{X_{obs}}\right)^2}$	[0, 1]	1
MAE	$MAE = \frac{1}{n}\sum_{i=1}^{n} \mid X_{obs}^{i} - X_{sim}^{i} \mid$	[0, +∞)	0
RMSE	$RMSE = \sqrt{\frac{\sum_{1}^{n}(sim_i - obs_i)^2}{n}}$	[0, +∞)	0

4. Discussion

4.1. Observational Evidence of Climate Warming and Wetting

The Arid Area of Northwest China (AANC) is one of the world's most climate-sensitive inland regions, and its widely discussed "warming and wetting" phenomenon has remained controversial for decades. Much of this debate arises from differences in analysis periods, spatial coverage, and the drought metrics used across studies. Based on observations from 114 meteorological stations from 1962 to 2021, this study detected two clear climatic transition years—1987 for precipitation and 1997 for temperature—after which both variables exhibited accelerated and persistent increases. These findings corroborate previous regional studies, suggesting that a general warming–humidification tendency has indeed occurred since the late 20th century [48].

However, our multi-scale SPEI results reveal a more complex hydroclimatic evolution. After 1997, both drought frequency and intensity increased significantly, particularly at short and intermediate accumulation scales, indicating a shift from wetting to drying conditions. This apparent contradiction can be explained by the rapidly rising evaporative demand associated with warming. Although precipitation increased, it remains insufficient to offset enhanced evapotranspiration, resulting in amplified climatic water deficits. Thus, the observed "humidification" is more likely a transient feature superimposed on an inherently arid background rather than a fundamental hydroclimatic transition.

Historical drought records also support this interpretation, as the region experienced several severe drought episodes (e.g., 1978–1982; 1999–2001) during periods of rapid warming and anomalous atmospheric circulation. The combined evidence suggests that the AANC is currently entering a dual-phase regime characterized by warming-induced drying, greater interannual variability, and more frequent extreme hydrological events. These evolving conditions underscore the urgent need for adaptive water-resource strategies, integrated multi-sector climate planning, and enhanced drought early-warning systems under accelerated climate change [49].

4.2. Future Trends of Meteorological Drought

Climate model projections from CMIP6 under multiple Shared Socioeconomic Pathways (SSPs) generally support a continued warming–wetting tendency in Northwest China during the 21st century [50,51]. However, the direction and magnitude of future drought risk vary substantially depending on the drought index used. Indices relying solely on precipitation, such as the Standardized Precipitation Index (SPI), generally indicate wetter conditions [52]. In contrast, evapotranspiration-inclusive indices such as PDSI and SPEI consistently project increasing drought severity and spatial heterogeneity [53–55]. Our findings, based on multi-scale SPEI, align more closely with the latter, reinforcing the dominant role of warming-driven evaporative demand in shaping future hydroclimatic stress.

A key challenge in previous assessments lies in the sparse and uneven distribution of meteorological stations in the AANC, which contributes to substantial uncertainty. The region's complex climate drivers—including strong topographic gradients, glacier-

and snowmelt-fed hydrological systems, and desert–oasis land–atmosphere interactions—further complicate future drought projections [56,57].

To address these uncertainties, we developed a multi-model ensemble prediction framework that integrates complementary learning algorithms to improve robustness and generalization. The results indicate that, despite modest precipitation increases, drought severity will continue to intensify due to sustained warming and rising evaporative losses. By 2035, the AANC is projected to experience more frequent moderate-to-severe meteorological droughts, particularly at longer SPEI accumulation scales. These findings underscore that reliable drought prediction requires approaches accounting for nonlinear, multi-factor interactions rather than reliance on univariate precipitation metrics alone.

4.3. Innovation, Limitations, and Future Prospects

This study proposes an integrated Stacking ensemble learning framework that combines Elastic Net, Random Forest, and Prophet–XGBoost models for multi-scale meteorological drought prediction. Compared with single-model approaches, the Stacking framework offers several key advantages. Statistically, it stabilizes the hypothesis space and reduces generalization error; computationally, it mitigates local-optimum risks; and in terms of predictive skill, it captures both long-term tendencies and short-term anomalies more effectively. The improved statistical metrics (NSE = 0.886, MAE = 0.236, RMSE = 0.214) demonstrate the framework's strong capability for representing nonlinear temporal dynamics and extreme drought events.

Despite these strengths, several limitations remain. First, this study uses SPEI as the sole drought indicator, which primarily reflects meteorological drought. Future work should incorporate hydrological and agricultural drought indices and explicitly consider anthropogenic factors such as land-use change, groundwater extraction, irrigation intensity, and reservoir regulation [58–60]. Second, although the ensemble integrates three representative learning algorithms, other advanced models—such as Long Short-Term Memory (LSTM) networks, attention-based Transformers, and hybrid physical–statistical models—may further enhance long-term dependency capture and interpretability [61–63]. Building a larger multi-paradigm model library would improve transferability across regions and climate regimes. Third, the current framework is predominantly data-driven. Coupling machine-learning prediction with physically based hydrological or land-surface models could strengthen mechanistic understanding and improve scenario-based assessments.

Overall, the Stacking ensemble framework proposed here provides a valuable methodological advance for drought prediction in data-scarce arid regions. It highlights the dominant role of warming-induced evaporative demand in offsetting precipitation gains and offers a robust basis for improving drought preparedness, water-resource allocation, and climate adaptation strategies under continued global warming.

5. Conclusions

This study investigated the evolution and future projection of meteorological drought in the Arid Area of Northwest China (AANC) from 1962 to 2035 by integrating climatic trend analysis with multi-model ensemble learning. Using the BEAST algorithm, the temperature and precipitation series were decomposed to extract long-term trends and abrupt changes, revealing an overall warming and humidification pattern with significant shifts in 1987 and 1997. However, when evapotranspiration effects were incorporated through multi-scale SPEI analysis, the results indicated a transition from wetting to drying after 1997, suggesting that intensified warming has offset the humidification effect of precipitation. Among individual prediction models, Elastic Network and Random Forest captured partial trend and periodicity features but performed poorly for extreme values, whereas

Prophet combined with XGBoost better reproduced short-term fluctuations. The Stacking ensemble model, integrating the strengths of these learners, substantially improved prediction performance (NSE = 0.886, MAE = 0.236, RMSE = 0.214) and exhibited stable residual behavior. Future projections show that the AANC will face increasing drought severity by 2035, with higher uncertainty and a greater likelihood of extreme droughts at longer time scales. These findings enhance the understanding of warming-induced drought intensification and provide a robust methodological framework for drought prediction, water resource management, and climate adaptation planning in arid regions under future climate change.

Author Contributions: Conceptualization, T.P.; methodology, T.P.; software, T.P.; validation, T.P.; formal analysis, T.P. and J.W.; investigation, T.P.; resources, Y.W. and Y.C.; data curation, T.P. and M.F.; writing—original draft preparation, T.P.; writing—review and editing, Y.W. and Y.C.; visualization, Y.W.; supervision, Y.W. and Y.C.; project administration, Y.W. and Y.C.; funding acquisition, Y.W. and Y.C. All authors have read and agreed to the published version of the manuscript.

Funding: This research was supported by the National Natural Science Foundation of China, grant number W2412135; Natural Science Foundation of Xinjiang Uygur Autonomous Region, grant number 2024D01B85.

Data Availability Statement: Data will be made available on request.

Acknowledgments: We are sincerely grateful to the reviewers and editors for their constructive comments for the improvement of the manuscript.

Conflicts of Interest: The authors declare no conflict of interest.

References

1. Qing, Y.; Wang, S.; Yang, Z.L.; Gentine, P. Soil Moisture−Atmosphere Feedbacks Have Triggered the Shifts from Drought to Pluvial Conditions since 1980. *Commun. Earth Environ.* **2023**, *4*, 254. [CrossRef]
2. Wang, J.Y.; Li, Z.; Chen, Y.N. The Spatiotemporal Evolution of Socioeconomic Drought in the Arid Area of Northwest China Based on the Water Poverty Index. *J. Clean. Prod.* **2023**, *401*, 136719. [CrossRef]
3. Weng, Z.; Niu, J.; Guan, H.D.; Kang, S.Z. Three-Dimensional Linkage between Meteorological Drought and Vegetation Drought across China. *Sci. Total Environ.* **2023**, *859*, 160300. [CrossRef]
4. Wang, H.; Zhao, H.; Wang, F.Q.; Yan, B.; Tang, L.; Du, Y.T.; Cui, L.B. Study on the Multi-Type Drought Propagation Process and Driving Factors on the Tibetan Plateau. *J. Hydrol.* **2024**, *645*, 132162. [CrossRef]
5. Spinoni, J.; Barbosa, P.; Bucchignani, E.; Cassano, J.; Cavazos, T.; Christensen, J.H.; Christensen, O.B.; Coppola, E.; Evans, J.; Geyer, B.; et al. Future Global Meteorological Drought Hot Spots: A Study Based on CORDEX Data. *J. Clim.* **2020**, *33*, 3635–3661. [CrossRef]
6. Kwak, J.; Joo, H.; Jung, J.; Lee, J.; Kim, S.; Kim, H.S. A Case Study: Bivariate Drought Identification on the Andong Dam, South Korea. *Stoch. Environ. Res. Risk Assess.* **2021**, *35*, 549–560. [CrossRef]
7. Wang, T.; Tu, X.; Singh, V.P.; Chen, X.; Lin, K. Global Data Assessment and Analysis of Drought Characteristics Based on CMIP6. *J. Hydrol.* **2021**, *6*, 126091. [CrossRef]
8. Liu, Y.; Chen, J. Future Global Socioeconomic Risk to Droughts Based on Estimates of Hazard, Exposure, and Vulnerability in a Changing Climate. *Sci. Total Environ.* **2021**, *751*, 142159. [CrossRef]
9. Zhou, Z.; Shi, H.; Fu, Q.; Ding, Y.; Li, T.; Liu, S. Investigating the Propagation from Meteorological to Hydrological Drought by Introducing the Nonlinear Dependence with Directed Information Transfer Index. *Water Resour. Res.* **2021**, *57*, e2021WR030028. [CrossRef]
10. Zhou, Z.Q.; Wang, P.; Li, L.Q.; Fu, Q.; Ding, Y.B.; Chen, P.; Xue, P.; Wang, T.; Shi, H.Y. Recent development on drought propagation: A comprehensive review. *J. Hydrol.* **2024**, *645*, 132196. [CrossRef]
11. Seneviratne, S.; Zhang, X.; Adnan, M.; Badi, W.; Dereczynski, C.; Luca, A.D.; Ghosh, S.; Iskandar, I.; Kossin, J.; Lewis, S.; et al. Weather and Climate Extreme Events in a Changing Climate. In *Climate Change 2021: The Physical Science Basis*; IPCC, Ed.; Cambridge University Press: Cambridge, UK, 2021.
12. Zhu, Z.Y.; Duan, W.L.; Zou, S.; Zeng, Z.Z.; Chen, Y.N.; Feng, M.Q.; Qin, J.X.; Liu, Y.C. Spatiotemporal Characteristics of Meteorological Drought Events in 34 Major Global River Basins during 1901–2021. *Sci. Total Environ.* **2024**, *921*, 170913. [CrossRef] [PubMed]

13. Zhao, Y.Y.; Ma, E.Z.; Zhou, Z.Q.; Zou, Y.G.; Cao, Z.D.; Cai, H.J.; Li, C.; Yan, Y.H.; Chen, Y. Detecting the Non-separable Causality in Soil Moisture-Precipitation Coupling with Convergent Cross-Mapping. *Water Resour. Res.* **2024**, *60*, e2023WR034616. [CrossRef]
14. Zhao, Y.Y.; Zhu, T.J.; Zhou, Z.Q.; Cai, H.J.; Cao, Z.D. Detecting Nonlinear Information about Drought Propagation Time and Rate with Nonlinear Dynamic System and Chaos Theory. *J. Hydrol.* **2023**, *623*, 129810. [CrossRef]
15. Zhang, X.; Hao, Z.C.; Singh, V.P.; Zhang, Y.; Feng, S.F.; Xu, Y.; Hao, F.H. Drought Propagation under Global Warming: Characteristics, Approaches, Processes, and Controlling Factors. *Sci. Total Environ.* **2022**, *838*, 156021. [CrossRef]
16. Wei, X.; Huang, S.; Huang, Q.; Liu, D.; Leng, G.; Yang, H.; Duan, W.; Li, J.; Bai, Q.; Peng, J. Analysis of Vegetation Vulnerability Dynamics and Driving Forces to Multiple Drought Stresses in a Changing Environment. *Remote Sens.* **2022**, *14*, 4231. [CrossRef]
17. Warter, M.M.; Singer, M.B.; Cuthbert, M.O.; Roberts, D.; Caylor, K.K.; Sabathier, R.; Stella, J. Drought Onset and Propagation into Soil Moisture and Grassland Vegetation Responses during the 2012–2019 Major Drought in Southern California. *Hydrol. Earth Syst. Sci.* **2021**, *25*, 3713–3729. [CrossRef]
18. Wang, X.J.; Zhang, B.Q.; Zhang, Z.Y.; Tian, L.; Kunstmann, H.; He, C.S. Identifying Spatiotemporal Propagation of Droughts in the Agro-Pastoral Ecotone of Northern China with Long-Term WRF Simulations. *Agric. For. Meteorol.* **2023**, *336*, 109474. [CrossRef]
19. Vicente-Serrano, S.M.; Quiring, S.M.; Peña-Gallardo, M.; Yuan, S.S.; Domínguez-Castro, F. A Review of Environmental Droughts: Increased Risk under Global Warming? *Earth-Sci. Rev.* **2020**, *201*, 102953. [CrossRef]
20. Duan, R.; Huang, G.; Wang, F.; Tian, C.; Wu, X. Observations over a Century Underscore an Increasing Likelihood of Compound Dry-hot Events in China. *Earths Future* **2024**, *12*, e2024EF004546. [CrossRef]
21. Wu, Z.; Yin, H.; He, H.; Li, Y. Dynamic-LSTM Hybrid Models to Improve Seasonal Drought Predictions over China. *J. Hydrol.* **2022**, *615*, 128706. [CrossRef]
22. Ji, P.; Su, R.; Wu, G.; Xue, L.; Zhang, Z.; Fang, H.; Gao, R.; Zhang, W.; Zhang, D. Projecting Future Wetland Dynamics Under Climate Change and Land Use Pressure: A Machine Learning Approach Using Remote Sensing and Markov Chain Modeling. *Remote Sens.* **2025**, *17*, 1089. [CrossRef]
23. Ding, Y.; Yu, G.; Tian, R.; Sun, Y. Application of a Hybrid CEEMD-LSTM Model Based on the Standardized Precipitation Index for Drought Forecasting: The Case of the Xinjiang Uygur Autonomous Region, China. *Atmosphere* **2022**, *13*, 1504. [CrossRef]
24. Sabzipour, B.; Arsenault, R.; Troin, M.; Martel, J.-L.; Brissette, F.; Brunet, F.; Mai, J. Comparing a long short-term memory (LSTM) neural network with a physically-based hydrological model for streamflow forecasting over a Canadian catchment. *J. Hydrol.* **2023**, *627*, 130380. [CrossRef]
25. Li, Q.; Wang, Z.; Shangguan, W.; Li, L.; Yao, Y.; Yu, F. Improved daily SMAP satellite soil moisture prediction over China using deep learning model with transfer learning. *J. Hydrol.* **2021**, *600*, 126698. [CrossRef]
26. Majhi, B.; Naidu, D.; Mishra, A.P.; Satapathy, S.C. Improved Prediction of Daily Pan Evaporation Using Deep-LSTM Model. *Neural Comput. Appl.* **2020**, *32*, 7823–7838. [CrossRef]
27. Silini, R.; Masoller, C. Fast and Effective Pseudo Transfer Entropy for Bivariate Data-Driven Causal Inference. *Sci. Rep.* **2021**, *11*, 8423. [CrossRef] [PubMed]
28. Shi, H.Y.; Zhao, Y.Y.; Liu, S.N.; Cai, H.J.; Zhou, Z.Q. A New Perspective on Drought Propagation: Causality. *Geophys. Res. Lett.* **2022**, *49*, e2021GL096758. [CrossRef]
29. Pan, C.; Li, R.; Hu, Q.; Niu, C.; Liu, W.; Lu, W. Contrastive Learning Network Based on Causal Attention for Fine-Grained Ship Classification in Remote Sensing Scenarios. *Remote Sens.* **2023**, *15*, 3393. [CrossRef]
30. Wang, Y.; Liu, Z.; Li, J.; Lin, H.; Long, J.; Mu, G.; Li, S.; Lv, Y. Individual Tree-Level Biomass Mapping in Chinese Coniferous Plantation Forests Using Multimodal UAV Remote Sensing Approach Integrating Deep Learning and Machine Learning. *Remote Sens.* **2025**, *17*, 3830. [CrossRef]
31. Cao, W.; Fu, Y.; Cheng, Y.; Zhai, W.; Sun, X.; Ren, Y.; Pan, D. Modeling Potential Arsenic Enrichment and Distribution Using Stacking Ensemble Learning in the Lower Yellow River Plain, China. *J. Hydrol.* **2023**, *625*, 129985. [CrossRef]
32. Ding, X.; Feng, C.; Yu, P.; Li, K.; Chen, X. Gradient Boosting Decision Tree in the Prediction of NOx Emission of Waste Incineration. *Energy* **2023**, *264*, 126174. [CrossRef]
33. Ching, P.M.L.; Zou, X.; Wu, D.; So, R.H.Y.; Chen, G.H. Development of a Wide-Range Soft Sensor for Predicting Wastewater BOD Using an eXtreme Gradient Boosting (XGBoost) Machine. *Environ. Res.* **2022**, *210*, 112953. [CrossRef]
34. Sun, Z.X.; Zhao, M.Y.; Dong, Y.; Cao, X.; Sun, H.X. Hybrid Model with Secondary Decomposition, Random Forest Algorithm, Clustering Analysis and Long Short Memory Network Principal Computing for Short-Term Wind Power Forecasting on Multiple Scales. *Energy* **2021**, *221*, 119848. [CrossRef]
35. Xu, D.H.; Zhang, Q.; Ding, Y.; Huang, H.P. Application of a Hybrid ARIMA–SVR Model Based on the SPI for the Forecast of Drought—A Case Study in Henan Province, China. *J. Appl. Meteorol. Climatol.* **2020**, *59*, 1239–1259. [CrossRef]
36. Ding, X.Y.; Yu, Y.; Yang, M.L.; Wang, Q.; Zhang, L.Y.; Guo, Z.K.; Zhang, J.; Mailik, I.; Malgorzata, W.; Yu, R.D.; et al. Investigating the Effect of Climate Change on Drought Propagation in the Tarim River Basin Using Multi-Model Ensemble Projections. *Atmosphere* **2023**, *15*, 50. [CrossRef]

37. Li, Y.S.; Chen, Y.N.; Chen, Y.P.; Duan, W.L.; Wang, J.Y.; Wang, X. Characteristics of Dry and Wet Changes and Future Trends in the Tarim River Basin Based on the Standardized Precipitation Evapotranspiration Index. *Water* **2024**, *16*, 880. [CrossRef]
38. Cao, S.P.; Zhang, L.F.; He, Y.; Zhang, Y.L.; Chen, Y.; Yao, S.; Yang, W.; Sun, Q. Effects and Contributions of Meteorological Drought on Agricultural Drought under Different Climatic Zones and Vegetation Types in Northwest China. *Sci. Total Environ.* **2022**, *821*, 153270. [CrossRef]
39. Chen, W.; Li, Y.; Xue, W.; Shahabi, H.; Li, S.; Hong, H.; Wang, X.; Bian, H.; Zhang, S.; Pradhan, B.; et al. Modeling Flood Susceptibility Using Data-Driven Approaches of Naïve Bayes Tree, Alternating Decision Tree, and Random Forest Methods. *Sci. Total Environ.* **2020**, *701*, 134979. [CrossRef]
40. Hu, T.; Toman, E.M.; Chen, G.; Shao, G.; Zhou, Y.; Li, Y.; Zhao, K.; Feng, Y. Mapping Fine-Scale Human Disturbances in a Working Landscape with Landsat Time Series on Google Earth Engine. *ISPRS J. Photogramm. Remote Sens.* **2021**, *176*, 250–261. [CrossRef]
41. Vicente-Serrano, S.M.; Beguería, S.; López-Moreno, J.I. A Multiscalar Drought Index Sensitive to Global Warming: The Standardized Precipitation Evapotranspiration Index. *J. Clim.* **2010**, *23*, 1696–1718. [CrossRef]
42. Wang, E.; Huang, T.; Liu, Z.; Bao, L.; Guo, B.; Yu, Z.; Feng, Z.; Luo, H.; Ou, G. Improving Forest Above-Ground Biomass Estimation Accuracy Using Multi-Source Remote Sensing and Optimized Least Absolute Shrinkage and Selection Operator Variable Selection Method. *Remote Sens.* **2024**, *16*, 4497. [CrossRef]
43. Tay, J.K.; Narasimhan, B.; Hastie, T. Elastic Net Regularization Paths for All Generalized Linear Models. *J. Stat. Softw.* **2023**, *106*, 1–31. [CrossRef]
44. Breiman, L. Random Forests. *Mach. Learn.* **2001**, *45*, 5–32. [CrossRef]
45. Chen, T.; Guestrin, C. XGBoost: A Scalable Tree Boosting System. In Proceedings of the 22nd ACM SIGKDD International Conference on Knowledge Discovery and Data Mining, San Francisco, CA, USA, 13–17 August 2016; pp. 785–794.
46. Charoenkwan, P.; Chiangjong, W.; Nantasenamat, C.; Hasan, M.M.; Manavalan, B.; Shoombuatong, W. StackIL6: A Stacking Ensemble Model for Improving the Prediction of IL-6 Inducing Peptides. *Brief. Bioinform.* **2021**, *22*, bbab172. [CrossRef]
47. Lazzarini, R.; Tianfield, H.; Charissis, V. A Stacking Ensemble of Deep Learning Models for IoT Intrusion Detection. *Knowl.-Based Syst.* **2023**, *279*, 110941. [CrossRef]
48. Chen, F.; Xie, T.; Yang, Y.; Chen, S.; Chen, F.; Huang, W.; Chen, J. Discussion of the "Warming and Wetting" Trend and Its Future Variation in the Drylands of Northwest China under Global Warming. *Sci. China Earth Sci.* **2023**, *66*, 1241–1257. [CrossRef]
49. Li, Z.; Liu, H.H. Temporal and Spatial Variations of Precipitation Change from Southeast to Northwest China during the Period 1961–2017. *Water* **2020**, *12*, 2622. [CrossRef]
50. Yao, J.Q.; Zhao, Y.; Chen, Y.N.; Yu, X.J.; Zhang, R.B. Multi-Scale Assessments of Droughts: A Case Study in Xinjiang, China. *Sci. Total Environ.* **2018**, *630*, 444–452. [CrossRef]
51. Zhu, X.; Lee, S.Y.; Wen, X.H.; Ji, Z.M.; Lin, L.; Wei, Z.G.; Zheng, Z.Y.; Xu, D.Y.; Dong, W.J. Extreme climate changes over three major river basins in China as seen in CMIP5 and CMIP6. *Clim. Dyn.* **2021**, *57*, 1187–1205. [CrossRef]
52. Qin, J.; Su, B.; Tao, H.; Wang, Y.; Huang, J.; Li, Z.; Jiang, T. Spatio-Temporal Variations of Dryness/Wetness over Northwest China under Different SSPs-RCPs. *Atmos. Res.* **2021**, *259*, 105672. [CrossRef]
53. Yang, P.; Xia, J.; Zhan, C.S.; Zhang, Y.Y.; Hu, S. Discrete Wavelet Transform-Based Investigation into the Variability of Standardized Precipitation Index in Northwest China during 1960–2014. *Theor. Appl. Climatol.* **2018**, *132*, 167–180. [CrossRef]
54. Wang, Z.; Li, J.; Lai, C.; Zeng, Z.; Zhong, R.; Chen, X.; Zhou, X.; Wang, M. Does Drought in China Show a Significant Decreasing Trend from 1961 to 2009? *Sci. Total Environ.* **2017**, *579*, 314–324. [CrossRef] [PubMed]
55. Huang, W.; Liu, C.; Cao, J.Q.; Chen, J.H.; Feng, S. Changes of Hydroclimatic Patterns in China in the Present Day and Future. *Sci. Bull.* **2020**, *65*, 1061–1063. [CrossRef] [PubMed]
56. Trepel, J.; le Roux, E.; Abraham, A.J.; Buitenwerf, R.; Kamp, J.; Kristensen, J.A.; Tietje, M.; Lundgren, E.J.; Svenning, J.C. Meta-Analysis Shows that Wild Large Herbivores Shape Ecosystem Properties and Promote Spatial Heterogeneity. *Nat. Ecol. Evol.* **2024**, *8*, 705–716. [CrossRef]
57. Chen, C.; Schwarz, L.; Rosenthal, N.; Marlier, M.E.; Benmarhnia, T. Exploring Spatial Heterogeneity in Synergistic Effects of Compound Climate Hazards: Extreme Heat and Wildfire Smoke on Cardiorespiratory Hospitalizations in California. *Sci. Adv.* **2024**, *10*, eadj7264. [CrossRef]
58. Saha, A.; Pal, S.C. Spatio-Temporal Variation of Meteorological, Hydrological and Agricultural Drought Vulnerability: Insights from Statistical, Machine Learning and Wavelet Analysis. *Groundw. Sustain. Dev.* **2024**, *27*, 101380. [CrossRef]
59. Zhang, P.P.; Cai, Y.P.; Cong, P.T.; Xie, Y.L.; Chen, W.J.; Cai, J.Y.; Bai, X.Y. Quantitation of Meteorological, Hydrological and Agricultural Drought under Climate Change in the East River Basin of South China. *Ecol. Indic.* **2024**, *158*, 111304. [CrossRef]
60. Zhang, R.Q.; Shangguan, W.; Liu, J.J.; Dong, W.Z.; Wu, D.Y. Assessing Meteorological and Agricultural Drought Characteristics and Drought Propagation in Guangdong, China. *J. Hydrol. Reg. Stud.* **2024**, *51*, 101611. [CrossRef]
61. Tuğrul, T.; Hınıs, M.A.; Oruç, S. Comparison of LSTM and SVM Methods through Wavelet Decomposition in Drought Forecasting. *Earth Sci. Inform.* **2025**, *18*, 139. [CrossRef]

62. Salas-Martínez, F.; Márquez-Grajales, A.; Valdés-Rodríguez, O.A.; Palacios-Wassenaar, O.M.; Pérez-Castro, N. Prediction of Agricultural Drought Behavior Using the Long Short-Term Memory Network (LSTM) in the Central Area of the Gulf of Mexico. *Theor. Appl. Climatol.* **2024**, *155*, 7887–7907. [CrossRef]
63. Gupta, B.B.; Gaurav, A.; Attar, R.W.; Arya, V.; Bansal, S.; Alhomoud, A.; Chui, K.T. Advance Drought Prediction through Rainfall Forecasting with Hybrid Deep Learning Model. *Sci. Rep.* **2024**, *14*, 30459. [CrossRef] [PubMed]

Disclaimer/Publisher's Note: The statements, opinions and data contained in all publications are solely those of the individual author(s) and contributor(s) and not of MDPI and/or the editor(s). MDPI and/or the editor(s) disclaim responsibility for any injury to people or property resulting from any ideas, methods, instructions or products referred to in the content.